

Bonding and Molecular Environment Effects on Near-Infrared Optical Absorption Behavior in Nonlinear Optical Monoazo Chromophore–Polymer Materials

Richard R. Barto*

Department of Materials Science and Engineering, Stanford University, Stanford, California

Curtis W. Frank

Department of Chemical Engineering, Stanford University, Stanford, California

Peter V. Bedworth, Rebecca E. Taylor, William W. Anderson, and Susan Ermer

Lockheed Martin Space Systems Company, Advanced Technology Center, Palo Alto, California

Alex K.-Y. Jen, J. D. Luo, and Hong Ma

Department of Materials Science and Engineering, University of Washington, Seattle, Washington

Hong-Zhi Tang†

Department of Chemistry, North Carolina State University, Raleigh, North Carolina

Michael Lee‡

APIC Corporation, Culver City, California

Albert S. Ren

Arena Pharmaceuticals, Inc., 6166 Nancy Ridge Drive, San Diego, California 92121

Received January 5, 2006; Revised Manuscript Received August 5, 2006

ABSTRACT: The mono-azo dyes Disperse Red 1 and Disperse Red 19 have been studied for several years as chromophores in polymers for nonlinear optical properties. These materials are examined here for the effects of dye donor group esterification in guest–host systems and by dye–polymer covalent attachment on near-infrared absorption behavior. The dye–polymer systems DR1–acrylate, DR1–poly-4-vinylphenol, and DR19–aliphatic epoxy are characterized by UV–vis absorption spectroscopy and photothermal deflection spectroscopy as guest–host systems with and without esterification of the DR1 and DR19 ethanol –OH substituents in guest–host systems, and as covalently attached dye copolymers, as a function of dye concentration up to 1700 μmol per gram of polymer. Esterification is shown to be an effective route to reducing near-IR loss in DR1/acrylate guest–host materials at high concentrations and in DR19/epoxy guest–host materials at most concentrations. Dye–polymer covalent attachment is shown to be highly effective for minimizing near-IR loss in the two DR1–polymer materials at all concentrations and is shown to be effective for DR19–epoxy materials at higher concentrations. Charge-transfer formation and the distributions of dye–polymer and dye–dye orientation states play crucial roles in the loss behavior of these materials.

Introduction

We report on a systematic study of Disperse Red monoazo dyes incorporated into three unrelated aliphatic polymers, under three dye incorporation schemes: unmodified guest–host systems, esterified dye guest–host systems, and covalently attached dye–polymer systems. As was reported on for two previous studies of highly active nonlinear optical dye/polymer guest–host materials,^{1,2} we systematically vary dye concentration under each of these schemes and qualitatively assess the effects of polymer structure and dye incorporation scheme on molecular interaction mechanisms that influence the low energy

tail of the main dye absorption peak and concomitant effects on near-IR loss. In the previous two studies,^{1,2} we reported on near-IR loss behavior in dye–polymer guest–host materials based on FTC-like NLO dyes, showing effects of dye spacer length and polymer structure on solvatochromism and inhomogeneous broadening of the main dye electronic transition peak. These processes were shown to correlate with near-IR loss versus dye concentration behavior.

The number density of the highly polar chromophores incorporated into the polymer system is a key determinant of the E–O device sensitivity, which can be constrained by E–O attenuation due to dipole interactions on close approach³ or by dye solubility limits in the polymer, exacerbated by polarity mismatch between dye and polymer. To increase chromophore loading and alignment stability, researchers have investigated covalent attachment of the chromophore to the polymer as either

* Corresponding author. E-mail: rick.barto@lmco.com.

† Current address: The Molecular Foundry, Materials Science Division, Lawrence Berkeley National Laboratory, Berkeley, CA 94720.

‡ Current address: Quintessence Photonics Corporation, 15632 Roxford Street, Sylmar, CA 91342-1265.

a pendant group^{4–29} or a comonomer,^{30–44} cross-linking the active moiety into the polymer system,^{45–51} or constructing covalently self-assembled superlattice structures containing oriented chromophores.^{52–57} These approaches have had mixed success in improving chromophore loading and have frequently led to higher device insertion loss.

The near-IR spectral structure can provide a rich description of the relative contributions to absorption loss. One such class of contributions arises from weak sub-electronic bands due to donor–acceptor,^{58–63} acid–base,^{64,65} or charge-transfer complexes^{66–68} or defect states.^{69–73} Complexes associated with these states can arise from specific interactions between neighboring molecules, and the strength and breadth of these bands gives an indication of the distribution and relative population of such states. The shape, position, and magnitude of these states will have direct consequences on loss in the near-IR.⁷⁴ Another significant contribution to near-IR loss is Urbach tail broadening,⁷⁵ associated with sub-gap absorption in amorphous materials exhibiting an exponential band tail distribution given by

$$\alpha(E) = \alpha^0 e^{E/E_u} \quad (1)$$

where $\alpha(E)$ is a constant, $\alpha(E)$ is the absorption coefficient at energy E , and E_u is referred to as the Urbach energy and indicates the width of the exponential distribution. The Urbach width has a thermal contribution of magnitude ΔkT , as well as contributions from temperature-independent disorder and distribution of defects in the material.⁷⁶

In this study, we investigate three structural strategies for incorporation of an NLO dye system into polymers for spectral near-IR absorption loss behavior: (1) covalent attachment of the dye to the polymer as either a comonomer or a pendant group; (2) solution mixing of the unmodified dye as a guest in the polymer host; and (3) solution mixing of the dye as a guest in the polymer host, with substitution of potentially charge-transfer forming –OH groups on the dye by ester groups. The well-characterized monazo dyes 4-[ethyl(2-hydroxyethyl)amino]-4'-nitroazobenzene (Disperse Red 1, CAS 2872-52-8, Figure 1a) and 4'-[(*N,N*-dihydroxyethyl)amino]-4-nitroazobenzene (Disperse Red 19, CAS 2734-52-3, Figure 1b) copolymerized as a pendant group and as a comonomer, respectively. These dyes are close analogues of each other, differing only in the number of donor ethyl –OH groups, with Disperse Red 1 (DR1) possessing one –OH group and Disperse Red 19 (DR19) possessing two –OH groups. Their structures fall within the merocyanine class of NLO dyes, and their commercial availability makes them convenient for studies of optical loss behavior associated with different molecular bonding and polymer host environments.

DR1 is incorporated into two different polymers as a pendant group, poly(R-methacrylate) and poly(4-vinylphenol) (Figure 1i and j, respectively). The copolymer poly(DR1-methyl methacrylate) at 10 mer% DR1 has been widely studied and shown to exhibit relatively low absorption loss (<0.5 dB/cm⁷⁷). Preliminary UV–vis measurements indicated that poly(4-vinylphenol) (PVP) has high transparency in the visible to near-IR, and the acidic pendant –OH group lends itself to pendant dye attachment. DR19 is incorporated as a comonomer into a linear aliphatic Bisphenol A epoxy derivative, Bisphenol A *N*-hydroxyethyl ether-*N'*-ether-*co-N,N*-bis(2-hydroxypropyl)aniline (“epoxy”, Figure 1h). High transparency in the visible to near-IR was found for the neat epoxy derivative in initial UV–vis measurements. Each of these copolymers is investigated at three dye loading levels.

For each of the dye–polymer combinations discussed above for studies of covalently attached dyes, analogous guest–host materials are studied at comparable molar concentrations of dye, both for unmodified dye and with the –OH groups protected by esterification. For DR1/acrylate and DR19/epoxy systems, the –OH group is substituted with acetate (OAc), while for the DR1/PVP system, the –OH group is substituted with benzoate (OC₆H₅). The choice of –OH protecting groups in each dye–polymer system is intended to more closely mimic the molecular surroundings of the dye in the covalently attached state.

We show the benefits of covalent dye–polymer attachment in reducing near-IR loss in all of the dye–polymer systems, and effectiveness of dye donor group ester protection for reducing near-IR loss in DR1/acrylate and DR19/epoxy guest–host systems. Charge transfer is shown to be an important effect in DR1–PVP and, to a lesser extent, in DR19–epoxy systems. Urbach tail broadening is important for all systems studied.

Experimental Section

Materials Synthesis. Poly(Disperse Red 1 methacrylate-*co*-methyl methacrylate) at a Disperse Red 1 (DR1) doping level of 1010 μmol per gram of polymer (10 mer%) was received from IBM Almaden Research Labs and used as-received (CAS No. 119989-05-8, Figure 1a, with R = methyl, $M_w = 160\,000$, polydispersity 5, “DR1-acrylate”). The structure of unmodified poly(methyl methacrylate) is shown in Figure 2a, with R = –CH₂–.

Poly(DR1 methacrylate-*co*-ethyl methacrylate) at DR1 doping levels of 560 and 1710 μmol per gram of polymer (Figure 1a, with R = ethyl, “DR1-acrylate”) was prepared as follows. To the solution of DR1 (6.00 g, 18.1 mmol) in dry methylene chloride (20 mL) were added triethylamine (2.7 mL) and methacryloyl chloride (1.77 mL, 1.90 g, 18.1 mmol). The resulting mixture was stirred at room temperature for 4 h. The methylene chloride solution was extracted with water to remove water-soluble impurities. The crude DR1–acrylate monomer product was purified by silica gel chromatography eluting with hexane/methylene chloride (1:1 to 1:3) to afford a red solid (4.85 g, 70%). ¹H NMR (300 MHz, CDCl₃, ppm) δ : 1.27 (t, $J = 7.2$ Hz, 3H), 1.94–1.95 (m, 3H), 3.56 (q, $J = 7.5$ Hz, 2H), 3.74 (t, $J = 6.3$ Hz, 2H), 4.36 (t, $J = 6.3$ Hz, 2H), 5.60 (m, 1H), 6.11 (s, 1H), 6.83 (d, $J = 9.3$ Hz, 2H), 7.90 (d, $J = 6.6$ Hz, 2H), 7.93 (d, $J = 6.3$ Hz, 2H), 8.33 (d, $J = 9.3$ Hz, 2H).

Synthesis of DR1-Containing Poly(ethyl methacrylate)s. Polymerization of the monomer to form poly(ethyl methacrylate) (Figure 1i, R = –CH₂CH₂–) was carried out in dimethylformamide (DMF) solution under nitrogen atmosphere at 65 °C in the presence of 1 wt % 2,2'-azobisisobutyronitrile (AIBN) for 24 h. The resulting polymer solution was cooled and poured into methanol to precipitate the polymer. The precipitated polymer was filtered, redissolved and reprecipitated, filtered, and finally dried at 60 °C under reduced pressure overnight. This procedure yielded a copolymer containing 560 μmol of DR1 per gram of acrylate polymer ($M_w = 88\,700$, polydispersity 2.46). ¹H NMR (300 MHz, CDCl₃, ppm) δ : 0.87 (br), 1.03 (br), 1.24 (br), 1.81 (br), 1.91 (br), 3.53 (br), 3.70 (br), 4.02 (br), 4.14 (br), 6.81 (br), 7.89 (br), 8.31 (br). A second DR1–acrylate copolymer was prepared by this procedure at a dye concentration of 1710 μmol of DR1 per gram of acrylate polymer ($M_w = 74\,200$, polydispersity 2.50). ¹H NMR (300 MHz, CDCl₃, ppm) δ : 0.88 (br), 1.04 (br), 1.25 (br), 1.82 (br), 2.00 (br), 3.56 (br), 3.70 (br), 4.03 (br), 4.04 (br), 4.15 (br), 6.84 (br), 7.91 (br), 8.32 (br).

Poly(DR1 styrene-*co*-4-vinylphenol) (Figure 1j, “DR1–PVP”) was prepared at DR1 doping levels of 560, 1180, and 2120 μmol per gram of polymer via a Mitsunobu condensation between the pendant hydroxyl group on DR1 chromophore and the phenol group on poly-4-vinylphenol (PVP, Figure 1g). The loading level of the DR1 chromophore was estimated from the integration of the ¹H NMR spectra of the materials. All of the chemicals were purchased from Aldrich. For each composition (560, 1180, and 2120 μmol DR1 per gram of polymer), DR1 was recrystallized from acetone,

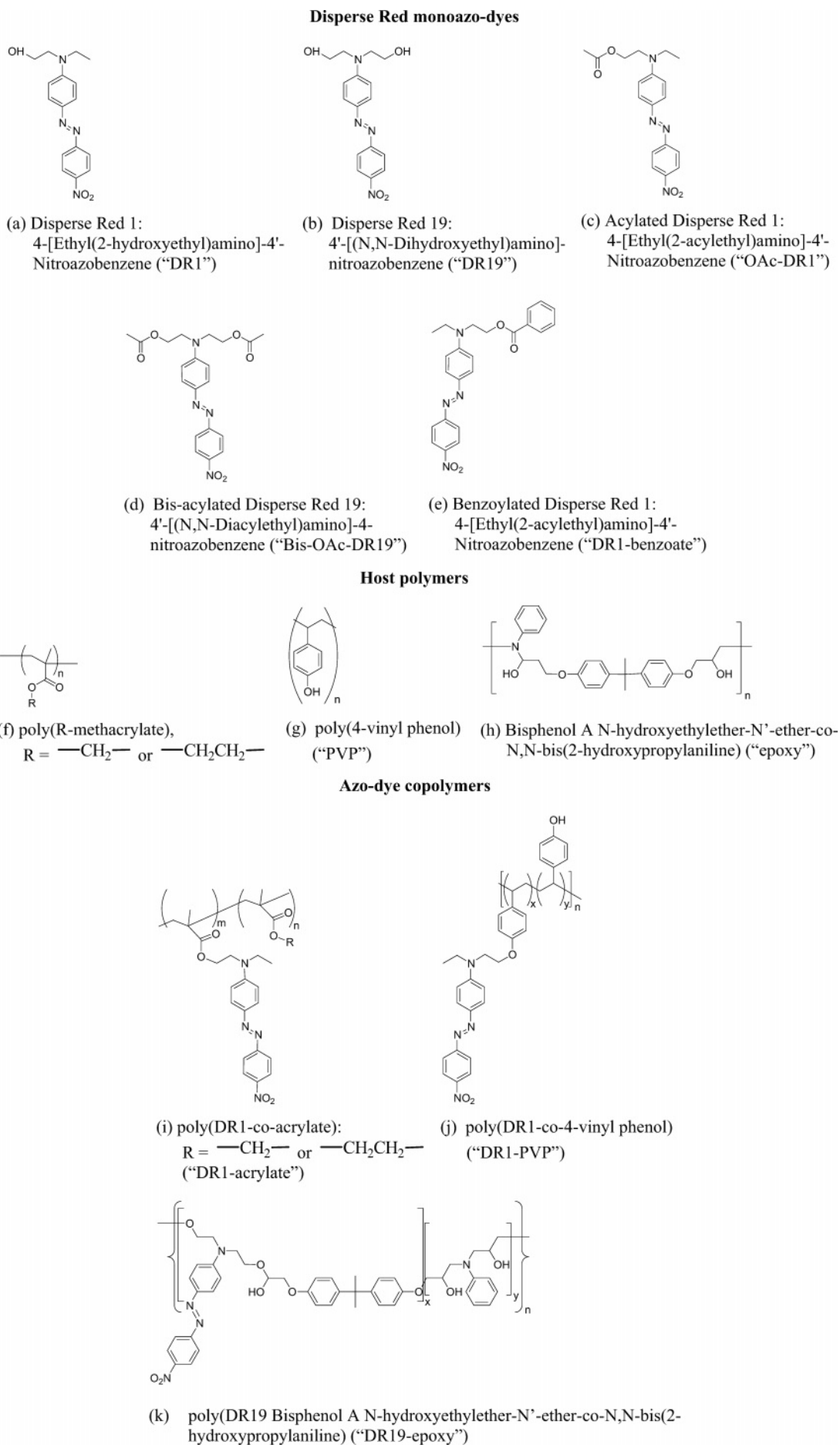


Figure 1. Monoazo guest dyes (a-e), host polymers (f-h), and azo dye copolymers (i-k) evaluated for this study.

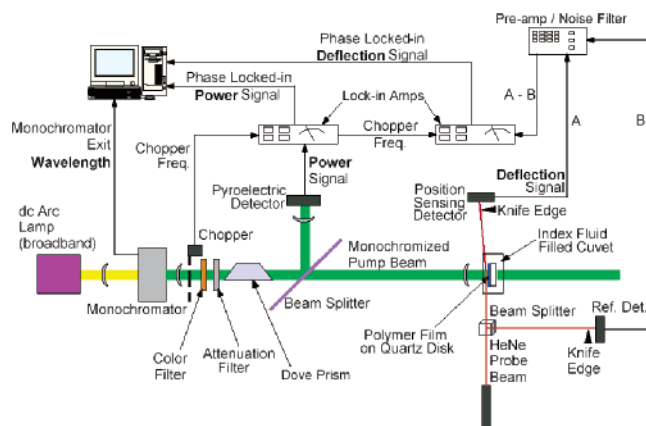


Figure 2. Schematic of PDS experimental configuration.

and tetrahydrofuran (THF) was distilled under nitrogen from sodium benzophenone ketyl prior to use. All of the other chemicals were used as received unless otherwise mentioned. To the THF solution of poly(4-vinylphenol) (1.0 g, 8.32 mmol), DR1 at appropriate molar quantities (0.636, 1.66, and 2.50 mmol, respectively, for 560, 1180, and 2120 $\mu\text{mol}/\text{gram}$), and triphenylphosphine (1.7:1 molar ratio to DR1) was added dropwise diethyl azodicarboxylate (DEAD, 1:1 molar ratio to triphenylphosphine). The reaction mixture was allowed to stir under nitrogen at room temperature for 36 h. The filtered solution was then added dropwise into diethyl ether. The collected red precipitation was further purified by Soxhlet extraction with methylene dichloride for 72 h and dried at 50 $^{\circ}\text{C}$ under vacuum overnight to afford the product as a red solid.

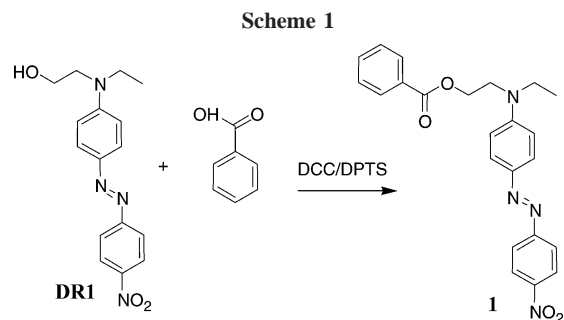
DR1–PVP (560 μmol DR1/g polymer). ^1H NMR (300 MHz, acetone- d_6 , ppm) δ : 8.27–8.42 (br s), 7.82–8.18 (br m), 6.2–7.13 (br, m), 4.06–4.33 (br s), 3.78–3.98 (br s), 3.53–3.74 (br s), 0.59–2.40 (br m). Molecular weight: $M_w = 27\,950$, polydispersity 2.05. UV–vis λ_{max} (in acetone): 480 nm.

DR1–PVP (1180 μmol DR1/g polymer). ^1H NMR (300 MHz, acetone- d_6 , ppm) δ : 8.23–8.46 (br s), 7.77–8.20 (br m), 6.16–7.17 (br, m), 4.01–4.31 (br s), 3.72–3.96 (br s), 3.43–3.71 (br s), 0.44–2.39 (br m). Molecular weight: $M_w = 23\,500$, polydispersity 1.87. UV–vis λ_{max} (in acetone): 483 nm.

DR1–PVP (2120 μmol DR1/g polymer). ^1H NMR (300 MHz, acetone- d_6 , ppm) δ : 8.15–8.40 (br s), 7.72–8.10 (br m), 6.17–7.09 (br m), 3.95–4.28 (br s), 3.36–3.93 (br m), 0.44–2.30 (br m). UV–vis λ_{max} (in acetone): 484 nm.

Poly(Disperse Red 19 Bisphenol A *N*-hydroxyethyl ether-*N'*-ether-*co-N,N*-bis(2-hydroxypropyl)aniline) (Figure 1k, “DR19–epoxy”) was prepared at DR19 doping levels of 530, 1010, and 1630 $\mu\text{mol}/\text{g}$ as follows. Epoxide functionalized Disperse Red 19 (DR19) chromophore was synthesized from the azo coupling reaction of *N,N*-bis(2,3-epoxypropyl)aniline and *p*-nitroaniline. Carefully matching the stoichiometry of epoxy groups, from epoxide–DR19 and Bisphenol A–diglycidyl ether, with the amine (from anilines), all monomers were dissolved in anhydrous dioxane in a drybox. The solution was heated to 90 $^{\circ}\text{C}$ and stirred for 30 min, and then heated to 110 $^{\circ}\text{C}$ for 36 h to complete polymerization in the drybox to form a linear epoxy polymer with loading of DR19 at 530, 1010, and 1630 $\mu\text{mol}/\text{g}$ (Figure 1k). Next, the solution was pumped down to remove the dioxane, the polymer was titrated with methanol 3X (until the methanol from the titration was clear), and the polymer product was thoroughly dried. The undoped linear Bisphenol A epoxy backbone polymer is depicted in Figure 1h. The weight-average molecular weight M_w of the epoxy backbone polymer was determined to be 10 300 by GPC against a polystyrene standard.

For evaluation of protected DR1/acrylate and protected DR19/epoxy guest–host materials, the ethanolamine moieties of DR1 and DR19 were esterified to form acetate-protected DR1 (Figure 1c) and DR19 analogues (Figure 1d). DR1 was used as received from Aldrich. DR19 was 1X recrystallized in acetone. To 1.5 mmol of DR1 or DR19 (0.5 g) were added 75.7 mmol of acetic anhydride



(7.1 mL) and 28.6 mL of anhydrous pyridine. The mixture was stirred overnight under an argon blanket, and then rotovapped at 40 $^{\circ}\text{C}$ for 1 h. The red crystalline crude product was washed with ethanol, and then heated into solution at 90 $^{\circ}\text{C}$ and filtered through a fritted filter funnel. The filtrate was dissolved in chloroform and 0.2 μm membrane filtered, followed by recrystallization in ethanol to form the purified product.

OAc-DR1. ^1H NMR (200 MHz, CDCl_3) δ : 8.33 (d, $J = 9.0$ Hz, 2H), 7.95–7.88 (m, 4H), 6.8 (d, $J = 9.0$ Hz, 2H), 4.30 (t, $J = 6.2$ Hz, 2H), 3.68 (t, $J = 6.0$ Hz, 2H), 3.50 (q, $J = 7.0$ Hz, 2H), 2.67 (s, 3H), 1.26 (t, $J = 7.0$ Hz, 3H).

Bis-OAc-DR19. ^1H NMR (200 MHz, $\text{DMSO}-d_6$) δ : 8.34 (d, $J = 8.8$ Hz, 2H), 7.92 (d, $J = 8.8$ Hz, 2H), 7.83 (d, $J = 8.8$ Hz, 2H), 6.97 (d, $J = 9$ Hz, 2H), 4.20 (br t, $J = 5.8$ Hz, 4H), 3.74 (br t, $J = 5.2$ Hz, 4H), 2.47 (br s, 6H).

For evaluation of benzoyl-protected DR1/PVP guest–host materials, the ethanolamine of DR1 was esterified with benzoate to form DR1-benzoate (Scheme 1). DR1 was received from Aldrich and recrystallized in acetone. Dichloromethane was distilled over phosphorus pentoxide, and THF was distilled over sodium/benzophenone prior to use. To the mixture of 1.0 g of DR1 (3.18 mmol) and 0.466 g of benzoic acid (Aldrich, 3.816 mmol) in dichloromethane/THF (2:1, v/v, 50 mL) were added 0.224 g of DPTS (4-(dimethylamino)-pyridinium 4-toluenesulfonate, 0.763 mmol) and then 0.866 g of DCC (1,3-dicyclohexylcarbodiimide, Aldrich, 4.197 mmol). The reaction mixture was allowed to stir at room temperature overnight. After filtration to remove the white precipitation of urea, the crude product (from the filtrate) was purified by column chromatography using dichloromethane/hexane as eluent (30:1, v/v) to afford 1.2 g of product (compound 1). ^1H NMR (200 MHz, CDCl_3 , ppm) δ : 8.32 (d, $J = 9.15$ Hz, 2H), 7.95–8.07 (m), 7.93 (d, $J = 8.78$ Hz, 2H), 7.92 (d, $J = 9.16$ Hz, 2H), 7.38–7.64 (m), 6.87 (d, $J = 9.16$ Hz, 2H), 4.55 (t, $J = 6.23$ Hz, 2H), 3.83 (t, $J = 6.22$ Hz, 2H), 3.60 (q, $J = 6.96$ Hz, 2H), 1.28 (t, $J = 6.96$ Hz, 3H).

Guest–Host Mixture Preparation. All solvents used in guest–host solutions were dried with molecular sieve. DR1 and DR19 from Aldrich were 1X recrystallized in acetone. With the exception of DR1/PVP and benzoyl-DR1/PVP guest–host solutions, all guest–host solutions were prepared as dilute solutions (low polymer solids contents in solvent), due to the generally poor solubility of the azo dyes. An exhaustive dye/polymer solubility screening study was performed in a wide range of solvents for each azo dye–polymer pair to determine solvent and concentrations at which stable solutions could be prepared.

DR1/PMMA guest–host solutions were prepared by adding DR1 to a dilute stock solution of PMMA (Scientific Polymer Products, CAS 9011-14-7, $M_w = 75\,000$) of 6.7 wt % polymer solids in *N*-methylpyrrolidone, at DR1 doping levels of 560, 1060, and 1710 μmol per gram of polymer.

DR1/PVP guest–host solutions were prepared by adding DR1 to a stock solution of PVP (Aldrich, CAS 24979-70-2, $M_w = 20\,000$) of 24.0 wt % polymer solids in a 3:1 by weight mixture of dimethylacetamide and cyclopentanone, at DR1 doping levels of 560, 1060, and 1710 μmol per gram of polymer.

DR19/epoxy guest–host solutions were prepared by adding DR19 to a dilute stock solution of the epoxy backbone polymer (Figure 1h, $M_w = 10\,300$) of 8.4 wt % polymer solids in

N-methylpyrrolidone, at DR19 doping levels of 530, 1010, and 1630 μmol per gram of polymer.

OAcDR1/PMMA guest–host solutions were prepared by adding OAcDR1 (Figure 1c) to a dilute stock solution of PMMA (Scientific Polymer Products, CAS 9011-14-7, $M_w = 75\,000$) of 6.7 wt % polymer solids in a 1:1 by weight mixture of dimethylformamide and cyclopentanone, at OAcDR1 doping levels of 560, 1060, and 1710 μmol per gram of polymer.

Benzoyl-DR1/PVP guest–host solutions were prepared by adding benzoyl-DR1 (compound 1) to a stock solution of PVP (Aldrich, CAS 24979-70-2, $M_w = 20\,000$) of 14.8 wt % polymer solids in a 11:7 by weight mixture of cyclopentanone and *N*-methylpyrrolidone, at benzoyl-DR1 doping levels of 420, 560, 1060, and 1720 μmol per gram of polymer. The 1720 $\mu\text{mol}/\text{gram}$ solution was diluted to 7 wt % polymer solids with 11:7 cyclopentanone:*N*-methylpyrrolidone and boiled for 5 s.

Bis-OAcDR19/epoxy guest–host solutions were prepared by adding bis-OAcDR19 (Figure 1d) to a dilute stock solution of the epoxy backbone polymer (Figure 1h, $M_w = 10\,300$) of 4.9 wt % polymer solids in *N*-methylpyrrolidone, at bis-OAcDR19 doping levels of 430, 540, 800, 1000, and 1300 μmol per gram of polymer.

Specimen Preparation. DR1-*co*-acrylate polymer spin solutions were prepared by dissolving the copolymers in a 3:1 by weight mixture of cyclopentanone and diglyme at 22 wt % polymer solids content. DR1-*co*-PVP polymer spin solutions were prepared by dissolving the copolymers in cyclopentanone at polymer solids contents of 22.1, 21.1, 20.1, and 18.1 wt % for attached DR1 loading levels of zero (undoped), 560, 1180, and 2120 μmol per gram of polymer, respectively. DR19-*co*-epoxy polymer spin solutions were prepared by dissolving the copolymers in cyclopentanone at polymer solids contents of 21.7, 34.1, 25.0, and 25.1 wt % for attached DR19 loading levels of zero (undoped), 530, 1010, and 1630 μmol per gram of polymer, respectively.

Film samples for PDS spectral characterization were prepared on 1" diameter \times 0.020" thick ultralow OH (<1 ppm) optical quality fused silica substrates. The substrates were pre-cleaned using a Piranha ($\text{H}_2\text{SO}_4:\text{H}_2\text{O}_2$) process. All dilute guest–host solutions (DR1/PMMA, OAcDR1/PMMA, DR19/epoxy, and bis-OAcDR19/epoxy at all dye concentrations, and benzoyl-DR1/PVP at a dye concentration of 1720 μmol per gram of polymer) were filtered in place at 0.2 μm , and cast by manual spreading 1–5 drops over the substrate surface. Each of these films was baked under flowing dry nitrogen in a dark box to remove the solvent immediately after spreading the solution, using a bake schedule involving a lower hold temperature of 100–130 $^\circ\text{C}$ for 1–2 min, ramping to an upper hold temperature in 2–4 min, dwelling at the upper temperature for 5–7 min, and then cooling to 50 $^\circ\text{C}$ in <3 min. The lower and upper bake temperatures, ramp times, and hold times are given for each dilute solution guest–host mixture in Table 1 of the Supporting Information.

This manually spreading deposition technique was developed in response to initial spin trials on silicon wafers, in which spun and baked Disperse Red/polymer guest–host films exhibited a combination of crystallites and thinning or poor wetting in the central regions of the film. The primary objective of the manual technique was to achieve a wetted film area of at least 8 mm \times 4 mm (slightly greater than the PDS pump beam projected image on the sample) or reasonable uniformity (<15% variation), and free of crystallites, voids, or significant "orange peel" surface texture. Film thickness was not tightly controlled by this process, other than holding it to <17 μm to maintain the condition of an optically and thermally thin film within the PDS thermo-optical model of Rosenzweig.⁷⁷ It was found through experimental trial and error that the manual spreading technique for these dilute guest–host solutions was better suited than conventional spin deposition to meet these film property objectives.

As an explanatory note, we have found experimentally over the course of over 200 spectral PDS measurements spanning a wide range of NLO dye polymer systems that for films greater than 0.2 μm in thickness and within the optically and thermally thin limit, differences in film thickness are inconsequential to the resultant

spectra as long as the film morphology remains amorphous, defect free, and free of gross surface undulations. These conditions are generally met by films <20 μm thick with reasonable near-IR transparency. For this study, the majority of the films prepared and characterized were <8 μm thick and all were held to <18 μm thick. Film thickness variation within a sample contributes to the systematic uncertainty in the PDS optical absorption coefficient measurement. The measured variation in film thickness was within the error limits of the PDS measurements shown in the error bars in the Results.

In a few special cases, the films were deposited in two or three successive sequences of spinning or manually spreading followed by baking to remove solvent to prevent crystallization of the dye out of solution with the polymer. The benzoylated-DR1/PVP guest–host solution doped at 1720 μmol dye per gram of polymer was highly crystallized when spun and baked using the 14.8 wt % polymer solids solution. A crystal-free film of this dye/polymer composition was prepared by diluting to 7 wt % polymer solids, spreading one drop (filtered at 0.2 μm) across the surface manually, baking per the schedule shown in Table 2 for this composition, and repeating the drop–spread–bake sequence twice. Bis-OAcDR19/epoxy guest–host films doped at 540 and 1000 μmol dye per gram of polymer were prepared by spinning and baking 2–4 drops of the 4.9 wt % solids solution (filtered at 0.2 μm) under conditions shown in Tables 1 and 2 of the Supporting Information, followed by manually spreading an additional 3–4 drops of solution (filtered at 0.2 μm) across the spun film, and baking under conditions shown in Table 1 of the Supporting Information.

While we did not perform surface analyses to investigate film forming kinetics under this successive manual deposition scheme, we speculate that the first deposition to form an ultrathin film on the substrate served to denature the substrate surface of defects that nucleate dye crystallites, and rendered the surface more hydrophobic for improved wetting in subsequent depositions. This first ultrathin layer (or first and second layers in the cases of three successive depositions) was likely disrupted by the subsequent deposition, but we assert that these one or two initial layers were very thin and acted as a sacrificial quasi-surfactant layer, such that the disruption in film thickness was comparable to natural film thickness variations.

Thicknesses of the films prepared by manual spreading of dilute solution were determined after PDS and UV–vis characterization using a Tencor Instruments Alpha-Step profilometer over at least two razor scratches in the area characterized by PDS, with a minimum of three thickness measurements taken for each sample. All films accepted for PDS characterization exhibited visual thickness and color uniformity, and lacked obvious microstructure (crystals or distinct phases). Thickness variation within a sample (standard deviation) for DR1/PMMA films ranged from 1.2% to 10.8%, with all but one sample having variation <5.4%. For OAcDR1/PMMA films, thickness variation within a sample ranged from 1.6% to 4.6%. DR19/epoxy films exhibited sample thickness variations ranging from 4.6% to 11.3%. Bis-OAcDR19/epoxy films had sample thickness variations ranging from 0.3% to 11.3%, with all but one sample showing variation <8%. Benzoyl-DR1/PVP films at 1720 μmol of dye per gram of PVP had sample thickness variations of 4.0% and 6.4%.

All remaining solutions were spun onto the substrate by filtering 4–8 drops in place at 0.2–0.45 μm , and spinning using a Headway Research 2-step spinning apparatus with a 2 s spread followed by a higher speed spin ranging from 10 to 60 s depending on the solution viscosity and wetting characteristics. Each of these films was baked under flowing dry nitrogen in a dark box to remove the solvent immediately after spreading the solution, using a bake schedule involving a lower hold temperature of 100–130 $^\circ\text{C}$ for 5 min, ramping to an upper hold temperature in 5 min, dwelling at the upper temperature for 5 min, then cooling to 50 $^\circ\text{C}$ in <3 min. The spread, spin speeds, and spin times used for the dye–polymer systems prepared by this procedure are summarized in Supporting Information Table 2, and lower and upper bake temperatures and times are summarized in Supporting Information Table 1.

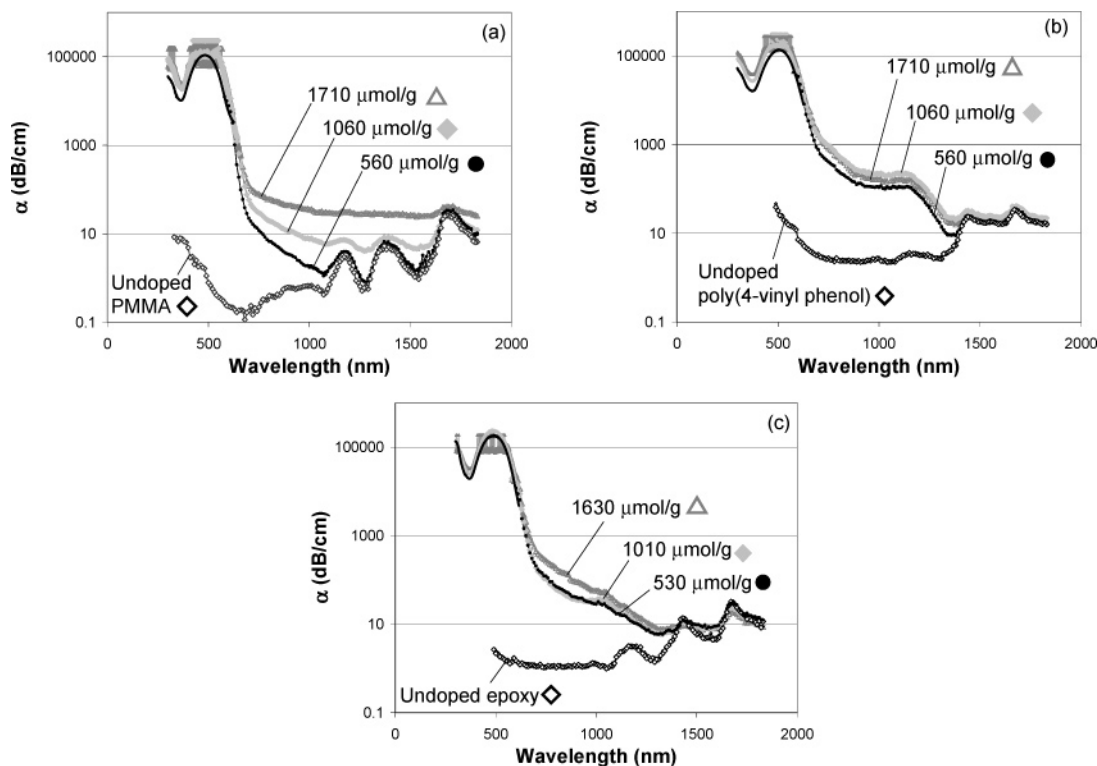


Figure 3. PDS spectral concentration series measured for azo dye–polymer guest host materials: (a) DR1/poly(methyl methacrylate); (b) DR1/poly(4-vinyl phenol); (c) DR109/linear aliphatic Bisphenol A epoxy.

All film samples were examined visually and at 50–200 \times , and judged to be of acceptable quality for PDS characterization if they exhibited thickness and color uniformity, and lacked obvious microstructure (crystals or distinct phases). Thicknesses of all spun samples were measured prior to PDS characterization by Alpha-Step over small razor scratches in two representative locations on each sample away from the center. Thicknesses of manually spread films ranged from 1.7 to 10 μm , while thicknesses of spun films ranged from 2 to 3.6 μm .

Spectroscopy. The principles of PDS were described in complete detail previously.¹ The PDS test bed used a 1 kW Hg(Xe) dc short arc lamp as the broadband illumination source at 12.6 Hz chopping frequency, with a 1/8 m dual-grating monochromator. The source beam image is a vertical ellipse, which is focused through vertical entrance slits to the monochromator at a divergence nearly matching that of the monochromator ($f/3.7$). To increase the length of interaction between the sample illuminated region and the probe beam, and thereby improve signal-to-noise, a Dove prism was used in the beam path (see Figure 2) to rotate the beam image by 90°, rendering it horizontal when focused onto the sample. A portion of the pump beam was split off and focused onto a pyroelectric detector to monitor optical power input at each wavelength via a lock-in amplifier. The probe beam was a 10 mW CW HeNe laser, attenuated to ~ 1.5 mW. The sample disk was mounted inside a fixture comprised of a back plate that slightly bends the vertical centerline of the sample into the probe beam. The fixtured sample was held inside a fused silica cuvette and filled with 3M Fluorinert Liquid FC-72 as the index fluid. The cuvette was closed with an O-ring sealed lid to prevent fluid evaporation. The cuvette was placed in a custom holder on a rotational translation stage attached to a triple axis translation stage, permitting precise alignment of the sample surface to the probe beam for maximized signal. Probe beam deflection was detected using a pn photodiode with an op-amp drive circuit providing gain and zero offset control. A blackened razor was used in front of the detector to shadow half of the probe beam. Half of the probe beam was split to a replicate reference detector prior to the sample. The primary and reference detector dc signals were conditioned with a preamplifier, with the difference signal forwarded to a second lock-in amplifier. This scheme provided cancellation of probe beam pointing noise.

PDS scans were performed by measuring deflection signal, input power, and phase lag at each wavelength, scanning from low energy to high energy in 10 nm increments. Low energy scans were performed first from 1830 nm to a minimum of 870 nm to reduce the possibility of photobleaching near the absorption maximum. A second, high energy scan was performed from 1830 to 600 nm for the dual purpose of finding the PDS saturated signal (strong absorption limit) and checking for any photobleaching effects from previous scans. A UV–vis absorption spectrum was collected in transmission mode on the same sample using a Cary 5E spectrophotometer, scanning from 1100 to 300 nm, to complete the optical absorption spectrum through the regions of overlap between PDS and Cary transmission data and the absorption maximum.

Results

DR1 and DR19 Polymer Guest–Host Mixtures. Representative UV–vis–PDS absorption spectra for the DR1/PMMA, DR1/PVP, and DR19/epoxy guest–host concentration series are shown in Figure 3a–c, respectively.

As seen in Figure 3a, extremely well-defined, sharp overtone peaks and very low near-IR loss values are seen for undoped PMMA (0.42, 0.51, and 0.94 dB/cm at 1060, 1300, and 1550 nm, respectively). The overtone peaks for DR1/PMMA at 560 μmol dye per gram of PMMA are equally sharp, with slight increases in loss (<0.6 dB/cm) at each wavelength. The overtone peaks are strongly attenuated at 1060 $\mu\text{mol/g}$ and are completely overwhelmed at 1710 $\mu\text{mol/g}$ by extreme Urbach tail broadening.

For DR1/PVP guest–host mixtures (Figure 3b), a distinct charge-transfer peak centered at 1140 nm is seen for all dye concentrations that is absent for undoped PVP. The shape of this charge-transfer (CT) band is invariant with concentration. This CT band controls near-IR loss at all concentrations at 1060 and 1300 nm, but at 1550 nm, loss appears to be controlled by a combination of the CT band and a strong, broad $\nu_{0,2}$ O–H overtone peak at 1440 nm seen for undoped PVP.

In Figure 3c, sharp overtone peaks are seen for undoped epoxy, with a moderate $\nu_{0,2}$ O–H overtone peak at 1440 nm

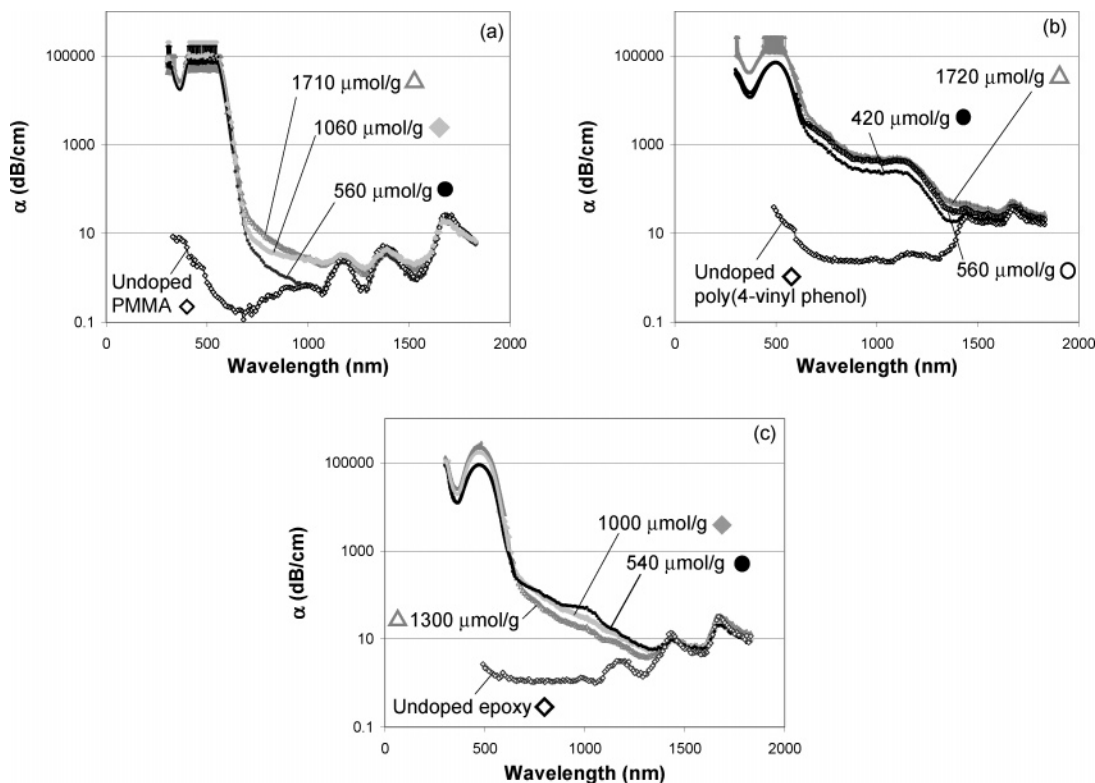


Figure 4. PDS spectral concentration series measured for acylated azo-dye-polymer guest host materials: (a) DR1-acetate/poly(methyl methacrylate); (b) DR1-benzoate/poly(4-vinyl phenol); (c) DR19-bis-acetate/linear aliphatic Bisphenol A epoxy.

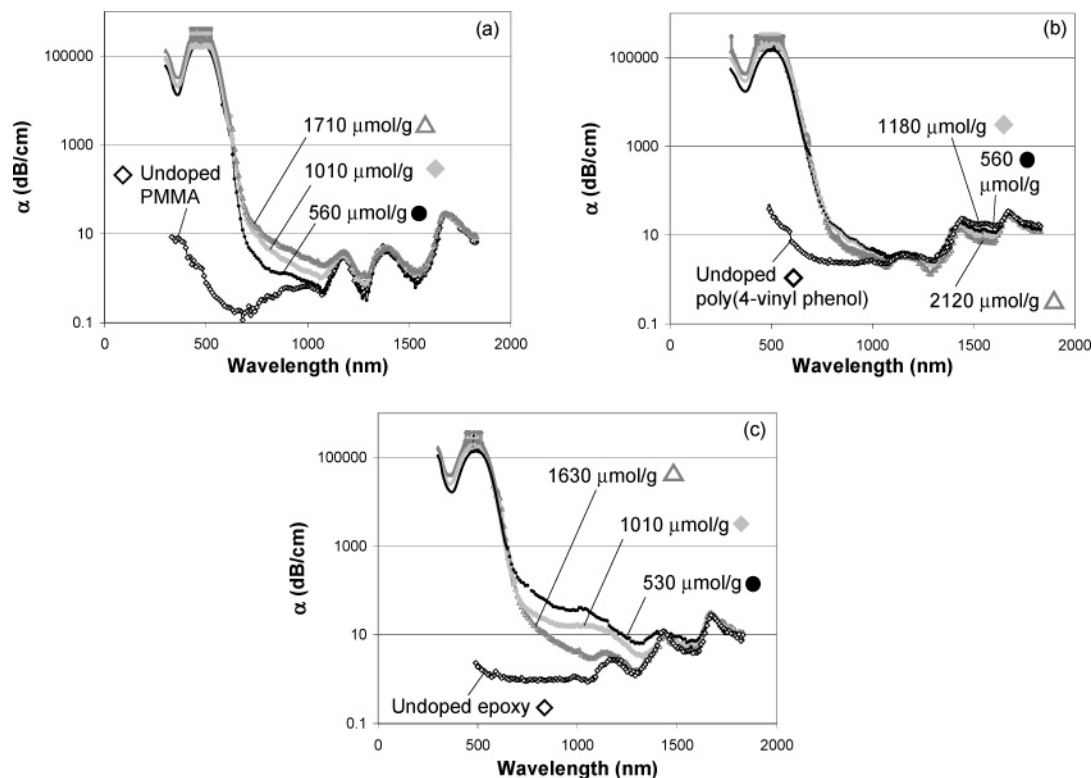


Figure 5. PDS spectral concentration series measured for azo-dye copolymers: (a) DR1-co-alkyl methacrylate; (b) DR1-co-4-vinyl phenol; (c) DR19-co-linear aliphatic Bisphenol A epoxy.

responsible for increased loss at 1550 nm relative to undoped PMMA, which is free of -OH . A broad CT band centered at ~ 1020 nm convolved with a broad Urbach tail is responsible for significant loss at 1060 and 1300 nm, and combines with the epoxy $\nu_{0,2}$ O-H overtone peak at 1440 nm to give larger loss at 1550 nm. Loss at 1060 and 1300 nm scales with the CT

intensity (highest at $1630 \mu\text{mol/g}$, lowest at $530 \mu\text{mol/g}$).

Esterified-DR1 and -DR19 Guest-Host Mixtures. Representative UV-vis-PDS absorption spectra for the acylated-DR1/PMMA, benzoated-DR1/PVP, bis-acylated-DR19/epoxy, and bis-acylated-DR19/PFC guest-host concentration series are shown in Figure 4a-d, respectively.

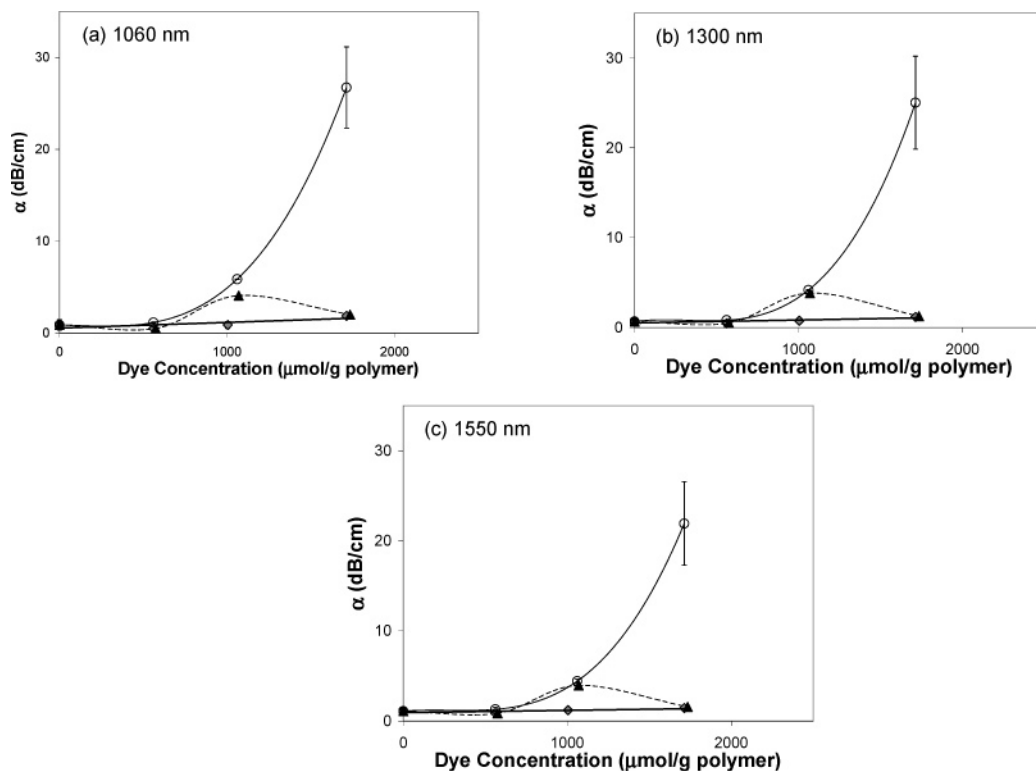


Figure 6. Disperse Red 1-acrylate polymer loss versus concentration trends at wavelengths of (a) 1060 nm; (b) 1300 nm; and (c) 1550 nm. \blacklozenge DR1-co-acrylate; \circ DR1/PMMA guest-host; \blacktriangle OAcDR1/PMMA guest-host.

For acylated-DR1/PMMA (Figure 4a), the sharp overtone peak structure and low near-IR loss for undoped PMMA is nearly replicated for DR1-acetate doping at 560 $\mu\text{mol/g}$. Near-IR loss at all concentrations is significantly lower than that of DR1/PMMA. Distinct Urbach tail broadening is seen at the intermediate concentration (1060 $\mu\text{mol/g}$), yielding near-IR loss greater than that seen at the highest concentration (1710 $\mu\text{mol/g}$).

The structure of the spectra for DR1-benzoate/PVP (Figure 4b) is nearly identical to that of DR1/PVP at all concentrations, indicating no apparent effect of benzylation on charge-transfer behavior for the DR1/PVP guest-host systems.

For DR19-bis-acetate/epoxy guest-host materials (Figure 4c), a CT band is convolved with an Urbach tail in all cases. The sharpest CT band occurs at the two lowest concentrations (430 and 540 $\mu\text{mol/g}$), yielding slightly higher loss at 1300 nm, but not at 1550 nm. Spectral structure and loss magnitudes at 1300 and 1550 nm are seen to be relatively insensitive to concentration for DR19-bis-acetate/epoxy.

Dye-Attached Polymers. Representative UV-vis-PDS absorption spectra for covalently attached DR1-acrylate, DR1-PVP, and DR19-epoxy concentration series are shown in Figure 7a–d, respectively.

Spectra for DR1-acrylate copolymers (Figure 5a) show sharp overtone peaks at all concentrations, with loss at each near-IR minimum (1060, 1300, 1550 nm) increasing progressively with concentration. With the exception of acylated DR1/PMMA at 560 $\mu\text{mol/g}$, the DR1-acrylate copolymer spectra exhibit the lowest near-IR loss values among all of the azo dye polymer systems studied. The main absorption peak shows no solvatochromism with increased concentration or with changing acrylate alkyl substituent length (R) and shows progressive broadening with concentration. For these reasons, the effect of acrylate substituent length on loss mechanisms is judged to be of little

consequence relative to DR1 ethanol –OH substitution or covalent attachment for purposes of evaluation.

Spectra for all DR1-PVP dye concentrations (Figure 5b) are free of CT bands, in contrast with DR1/PVP and DR1-acetate/PVP guest-host systems. Overtones for all DR1-PVP spectra are less well defined than for DR1-PMMA, and the main peak for DR1-PVP is red shifted by ~ 24 nm relative to DR1-PMMA at 560 $\mu\text{mol/g}$. This strong bathochromism, combined with a broader Gaussian main peak, is responsible for the higher observed loss at 1060 and 1300 nm in DR1-PVP relative to DR1-PMMA. Note that the DR1-PVP copolymers have equivalent or lower loss than undoped PVP. Loss at 1550 nm appears to be due to a combination of the strong $\nu_{0,2}$ O–H overtone peak at 1440 nm and solvatochromism in the main absorption peak. The DR1-PVP concentration series shows a downward progression of the near-IR loss minima at 1300 and 1550 nm with dye concentration. This appears to be due in part to a hypsochromic shift of the main absorption peak with increasing dye concentration. All of the broadening of the main absorption peak with increasing concentration occurs on the blue edge. The reduction in loss at 1550 nm with dye concentration appears to be due to a progressively less intense $\nu_{0,2}$ O–H overtone peak, which indicates a net reduction in the concentration of –OH moieties as DR1 concentration increases.

A prominent CT band is seen at ~ 1000 nm for DR19-epoxy at 530 $\mu\text{mol/g}$ (Figure 5c), which diminishes and red shifts to ~ 1110 nm at 1010 $\mu\text{mol/g}$, and completely disappears at 1630 $\mu\text{mol/g}$. Loss at all near-IR wavelengths (1060, 1300, 1550 nm) scales with the strength of the CT band and, as such, decreases with dye concentration from 530 to 1630 $\mu\text{mol/g}$.

Discussion

Loss versus concentration trends for each of the three molecular environments (guest-host, esterified guest-host, and

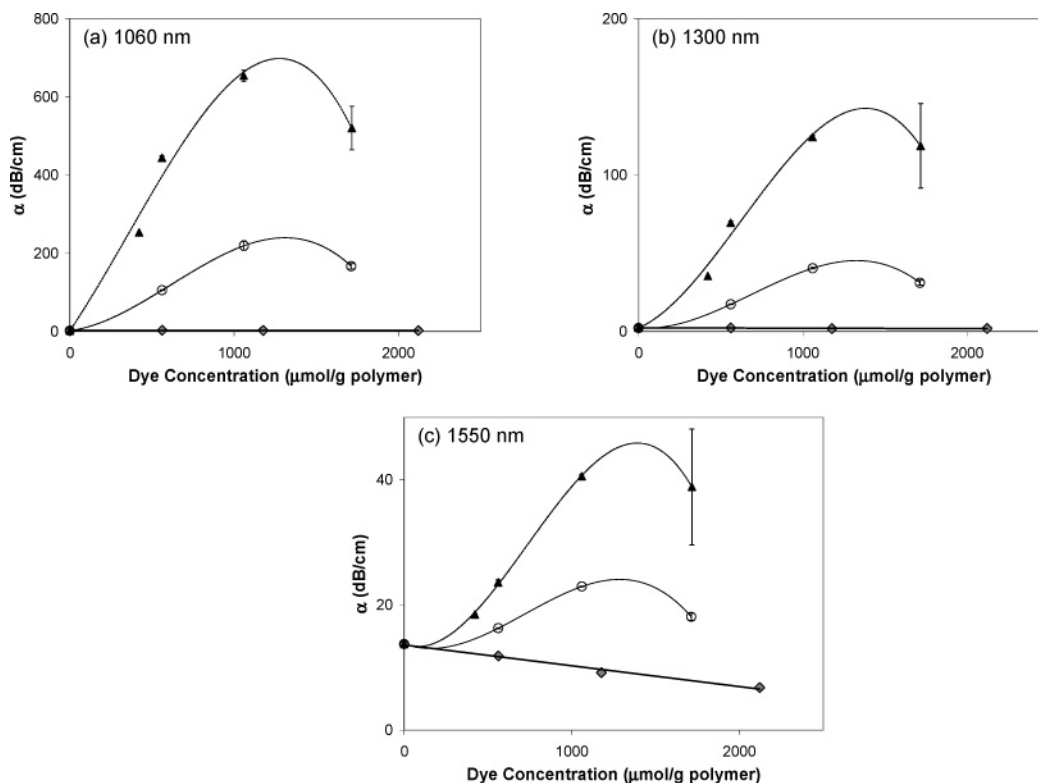


Figure 7. Disperse Red 1-PVP loss versus concentration trends at wavelengths of (a) 1060 nm; (b) 1300 nm; and (c) 1550 nm. \blacklozenge DR1-co-PVP; \circ DR1/PVP guest-host; \blacktriangle benzoyl-DR1/PVP guest-host.

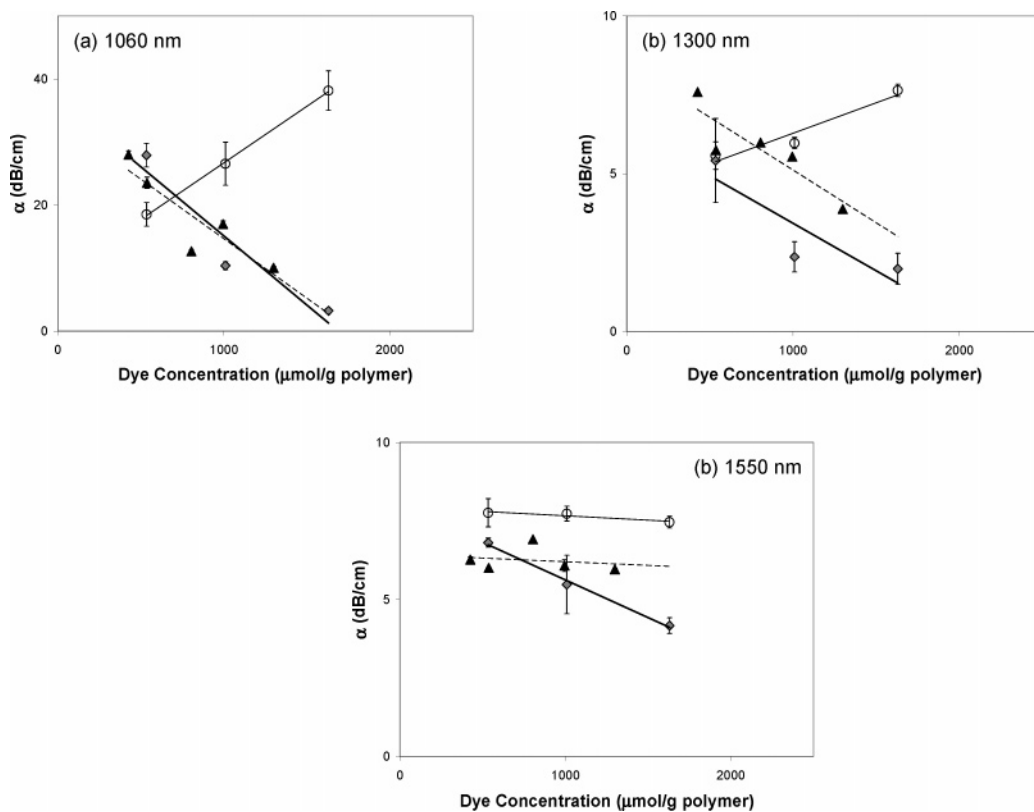


Figure 8. Disperse Red 19-epoxy loss versus concentration trends at wavelengths of (a) 1060 nm; (b) 1300 nm; and (c) 1550 nm. \blacklozenge DR19-co-epoxy; \circ DR19/epoxy guest-host; \blacktriangle bis-OAcDR19/epoxy guest-host. Curved lines are for visual guidance only.

covalently attached dye-polymer) are compared for each dye-polymer system in Figures 6–8 at wavelengths of 1060, 1300, and 1550 nm.

DR1-Acrylate Materials. For the DR1-acrylate system (Figure 6a–c, thick solid), covalent attachment is seen to yield

exceptionally low loss over all concentrations at each wavelength. The acylated DR1/PMMA guest-host materials exhibit loss values nearly equal to those of the covalently attached DR1-acrylate materials, except at intermediate concentration (1060 $\mu\text{mol/g}$), while the DR1/PMMA guest-host system shows

an exponential increase in loss with concentration, at each wavelength (Figure 6a–c, dashed).

The acylated DR1/PMMA system shows marked Urbach tail broadening at 1060 $\mu\text{mol/g}$ (Figure 4a), and this is seen to result in a slight increase in near-IR loss at this dye concentration. A proposed mechanism for the Urbach broadening at this concentration is dipole–dipole interactions between neighboring dye molecules that depend strongly on relative orientation. At the intermediate dye concentration, the acylated dye has sufficiently close average dye–dye spacing for dipole interactions to be important, with sufficient orientational freedom to take on a large distribution of dipole–dipole states. At higher concentration, the DR1–acetate molecules take on fewer orientations due to more localized ordering between the rigid molecules.

The exponential loss–concentration dependence observed for DR1/PMMA guest–host materials (Figure 6a–c, solid) is attributed to a broader distribution of dipole–induced dipole interactions between dye and polymer as concentration increases. Hydrogen bonding is ruled out in this system due to a lack of charge-transfer band structure in the spectra. The large reduction in loss at higher concentrations with both acylation and covalent attachment of DR1 provides evidence that the ethanol –OH on DR1 is responsible for a large broadening of the distribution of states between dye and polymer in the DR1/PMMA system, consistent with the progressive increase in Urbach tail width with concentration (Figure 3a). Acylation of DR1 as a means of reducing loss in this type of system is synthetically simpler than covalent attachment.

DR1–PVP Materials. For the DR1–PVP system, covalent attachment is clearly favored, showing a dramatic reduction in near-IR loss over the guest–host systems at each wavelength at all concentrations (Figure 7a–c, thick solid). Loss for the covalently attached materials has no concentration dependence at 1060 nm (Figure 7a, thick solid) and decreases linearly with concentration at 1300 and 1550 nm (Figure 7b and c, thick solid). More complex loss–concentration dependence is seen for both DR1/PVP and benzoylated-DR1/PVP guest–host systems, with an apparent loss maximum at $\sim 1350 \mu\text{mol/g}$ for both systems at each wavelength (Figure 7a–c). Benzoyl substitution of the DR1 ethanol –OH group in the guest–host system results in the largest values of loss at all concentrations among the DR1–PVP materials investigated, by orders of magnitude over DR1-co-PVP at 1060 and 1300 nm. Comparing the loss behavior of DR1/PVP guest–host systems (unprotected and ester protected) to that of DR1/acrylate, distinct charge-transfer (CT) behavior is seen in DR1/PVP while no CT is exhibited in DR1/acrylate. The carboxyl moiety of the acrylate backbone structure lacks sufficient electron-donating character to support a CT interaction with either DR1 or acylated DR1, while the acidic character of the phenol group in PVP gives rise to strong CT character with DR1 and DR1-benzoate. This CT character is greatly enhanced by the coplanarity of the DR1-benzoate and PVP phenol substituents. In contrast, esterification of DR1 reduces loss in the DR1/acrylate guest–host systems by sterically hindering the dye–polymer and dye–dye orientation states.

Losses measured for DR1/PVP guest–host materials are $\sim 1/4$ to $2/3$ the values measured for benzoylated-DR1 at all concentrations at each wavelength. The measured loss ratios between DR1/PVP and benzoylated-DR1/PVP guest–host systems at 1060 and 1300 nm are in agreement with ratios of charge-transfer band intensities at each concentration, in support of charge-transfer dominated near-IR loss for these systems at these

two wavelengths. Higher near-IR loss ratio of DR1/PVP to benzoylated-DR1/PVP seen at 1550 nm suggests that loss for DR1/PVP at this transmission band has a greater contribution from the intensity of the $\nu_{0,2}$ O–H overtone peak at 1440 nm than that contributed by the CT band.

The CT band in both guest–host systems occurs at the same energy (~ 1140 nm), but is ~ 3 times more intense for the benzoylated-DR1/PVP system. The occurrence of the CT band maximum at the same intermediate molar concentration in both systems suggests that the PVP phenol –OH group is responsible for the CT interaction with an electron-donating moiety on the dye. Steric hindrance to preferred orientation for CT is suggested for higher dye concentrations. Dye–polymer CT interaction appears to be significantly enhanced by the increased planarity of the dye donor group in the benzoylated-DR1/PVP system, as seen by the more intense CT band as compared to that of nonbenzoylated DR1/PVP, indicating a hydrogen bonding between the DR1 ethyl donor group (ethyl benzoate or ethanol) and the PVP phenol –OH in both guest–host systems. Quenching of the CT band seen in the covalently attached DR1–PVP system is most likely due to suppression of dye–polymer hydrogen bonding in this interaction scheme.

DR19–Epoxy Materials. The DR19–epoxy system shows advantages of both covalent incorporation of the dye into the polymer backbone and ester protection of the dye –OH groups in guest–host materials at all three near-IR transmission wavelengths, as compared to the nonacylated guest–host system (Figure 8). At concentrations from 430 to 1300 $\mu\text{mol/g}$, the bis-acylated-DR19/epoxy guest–host system exhibits loss decreasing linearly with concentration at 1060 and 1300 nm, but is nearly independent with concentration at 1550 nm. As seen in Figure 4c, this inverse linear loss–concentration dependence coincides with the relative strength of a broad CT band centered at ~ 1030 nm, convolved with a concentration-independent Urbach tail. The CT band intensity steadily decreases with concentration. This gradual reduction in loss and CT band strength with increasing dye concentration can be explained by a dye–polymer CT equilibrium that is first order in polymer concentration, that is, linearly inhibited by the addition of dye above 430 $\mu\text{mol/g}$. A likely dye–polymer interaction is CT between the epoxy alkyl –OH groups and the bis-ethyl acetate donor group of the dye. In this equilibrium, the dipole–dipole interaction between dye molecules increases linearly with dye concentration, proportionally decreasing the number of dye molecules available to the dye–polymer CT interaction.

The covalently attached DR19–epoxy system exhibits loss decreasing linearly with concentration at all three near-IR wavelengths over the concentration range 530–1630 $\mu\text{mol/g}$, and loss that is equivalent to or less than that measured for the bis-acylated-DR19/epoxy system at all wavelengths over most of the concentration range. As for the bis-acylated system, CT band intensity in attached DR19–epoxy decreases with concentration, and this dominates the net loss versus concentration trend.

These results show that CT in DR19–epoxy systems occurs in the absence of ethanol –OH groups (consistent with the CT bands observed in bis-acylated-DR19/epoxy) and is disrupted by the addition of dye (also consistent with the bis-acylated-DR19/epoxy results). At low dye concentration in attached DR19–epoxy, the dye has sufficient rotational freedom to form the dye–polymer charge-transfer interaction in attached DR19–epoxy. As concentration increases, the dye is more sterically hindered by other attached dye molecules to form the dye–polymer CT interaction, leading finally to CT quenching by

steric hindrance at high concentration (1630 $\mu\text{mol/g}$). Slight red-shifting of the CT band position with increased dye concentration suggests the CT interaction occurs in a more locally polar environment. Unlike bis-acylated-DR19/epoxy, covalent attachment of DR19 to the linear epoxy eliminates Urbach tail broadening, and at the highest concentration (1630 $\mu\text{mol/g}$), DR19–epoxy attachment eliminates charge transfer.

The unmodified DR19/epoxy guest–host system shows loss increasing linearly with concentration at 1060 and 1300 nm, opposite to the trends observed for copolymerized and acylated guest–host systems, while at 1550 nm, loss is relatively insensitive to concentration. As seen in Figure 3c, this loss–concentration dependence is due to a weak CT band centered at ~ 1020 nm that grows with increased concentration and that is convolved with broad Urbach tails. The CT band dominates loss magnitude at 1060 and 1300 nm, while at 1550 nm, the net loss is seen to be balanced between the CT band intensity and that of the $\nu_{0,2}$ O–H overtone peak at 1440 nm, which decreases with increasing DR19 concentration. The O–H overtone intensity decay with dye concentration shows that the number density of –OH moieties is controlled by the linear epoxy concentration. The concentration dependence of CT band strength and loss at 1060 nm and 1300 follows a CT equilibrium that is first order in dye concentration. Hydrogen bonding between the bis-ethanol –OH groups of DR19 and the epoxy alkyl –OH groups is limited by the relative abundance of more mobile DR19 –OH groups in this CT equilibrium.

The higher loss observed for the nonacylated DR19/epoxy guest–host system relative to attached- and acylated-DR19/epoxy at all concentrations (see Figures 3c vs 4c) is seen to derive from greater Urbach tail broadening due the smaller size of the unattached molecule, allowing it to take on more dye–dye and dye–polymer orientational states. DR19 acylation is therefore more effective in reducing loss in the guest–host epoxy as a result of increased steric hindrance to rotational and translational motion of the dye to reduce Urbach tail broadening. Covalent attachment of DR19 to epoxy has an even greater effect on reducing near-IR loss at high concentration, due to CT band quenching.

Comparing the loss behavior of DR19/epoxy systems to that of the two DR1/polymer guest–host systems (Figures 3–5), a less distinct CT band forms in DR19–epoxy in all bonding environments (guest–host, acylated guest–host, attached) and with less Urbach tail broadening. This band behavior suggests more restricted rotational and translational motion by the larger DR19 and DR19–acetate molecules relative to DR1.

Covalent attachment is shown to be less effective in quenching CT in DR19–epoxy as compared to that by DR1–PVP (Figure 5c and b, respectively). This is attributed to less restriction to rotational motion by double attachment in DR19–epoxy as compared to that by the phenyl group upon DR1 attachment to PVP.

Conclusions

The effects of nonlinear optical merocyanine azo dye donor group esterification and dye–polymer covalent attachment on dye–polymer spectral absorption behavior over the visible to near-IR was examined as a function of dye concentration for four dye–polymer systems.

Covalent attachment is seen to be an effective means to minimize near-IR absorption loss at all concentration in two DR1/polymer systems, that is, DR1–acrylate and DR1–polyvinylphenol (PVP), by restricting the number of dye–dye and dye–polymer orientational states in both polymers thereby

decreasing Urbach tail widths, and by quenching charge transfer in PVP. Covalent attachment was less effective in a DR19–epoxy system, due to less steric hindrance in doubly attached DR19 on the epoxy versus that by phenyl attachment in DR1–PVP, and due to a less homogeneous backbone structure in the epoxy versus acrylate and PVP.

Azo dye donor group esterification was effective in reducing near-IR loss in DR1/acrylate guest–host systems at high concentration, and in DR19/epoxy guest–host systems at most concentrations, due to steric hindrance of rotational and translational motion of the dye, restricting the number of dye–polymer and dye–dye orientational states and reducing Urbach tail width. Esterification of the DR1 donor group by benzoate in the DR1/PVP guest–host system sharply increased near-IR loss, due to charge-transfer enhancement by dye donor–polymer acceptor substituent coplanarity.

Characterization of spectral absorption behavior as a function of dye concentration is shown to be a valuable technique for gaining insights into the mechanisms responsible for near-IR loss in NLO azo-dye polymer materials.

Acknowledgment. R.R.B. gratefully acknowledges Lockheed Martin Corp. for financial support through the Lockheed Martin-Stanford Honors Co-op Program and Lockheed Martin independent research and development funding. R.R.B. would like to acknowledge Lawrence J. Dries, Dexter G. Girton, and Wendell D. Eades from Lockheed Martin, Andrew J. Skumanich from Applied Materials, and Carlton H. Seager from Sandia National Laboratories for significant technical guidance and many helpful discussions. Finally, we express sincere gratitude to Dr. Dan Dawson of IBM Almaden Research Labs for providing the 24% DR1–PMMA copolymer material, and to Prof. Shahin Maaref of Norfolk State University for providing recrystallized Disperse Red 19.

Supporting Information Available: Bake and spin conditions used for PDS film preparation. This material is available free of charge via the Internet at <http://pubs.acs.org>.

References and Notes

- (1) Barto, R. R.; Frank, C. W.; Bedworth, P. V.; Ermer, S.; Taylor, R. E. *J. Phys. Chem. B* **2004**, *108*, 8702.
- (2) Barto, R. R.; Frank, C. W.; Bedworth, P. V.; Ermer, S.; Taylor, R. E. *J. Chem. Phys.* **2005**, *122*, 234907/1.
- (3) Dalton, L. R.; Harper, A. W.; Robinson, B. H. *Proc. Natl. Acad. Sci. U.S.A.* **1997**, *94*, 4842.
- (4) DeMartino, R. N.; Choe, E. W.; Khanarian, G.; Haas, D.; Leslie, T.; Nelson, G.; Stamatoff, J.; Stuetz, D.; Teng, C. C.; Yoon, H. *Nonlinear Opt. Electroact. Polym.*, [*Proc. Am. Chem. Soc. Symp. Electroact. Polym.*] **1988**, 169.
- (5) DeMartino, R. N.; Allen, D. E.; Keosian, R.; Khanarian, G.; Haas, D. R. *Mater. Res. Soc. Symp. Proc.* **1992**, *228*, 39.
- (6) Ye, C.; Minami, N.; Marks, T. J.; Yang, J.; Wong, G. K. *Macromolecules* **1988**, *21*, 2899.
- (7) Ye, C.; Minami, N.; Marks, T. J.; Yang, J.; Wong, G. K. *NATO ASI Ser., Ser. E* **1989**, *162*, 173.
- (8) Li, D.; Minami, N.; Ratner, M. A.; Ye, C.; Marks, T. J.; Yang, J.; Wong, G. K. *Synth. Met.* **1989**, *28*, D585.
- (9) Hubbard, M. A.; Minami, N.; Ye, C.; Marks, T. J.; Yang, J.; Wong, G. K. *Proc. SPIE-Int. Soc. Opt. Eng.* **1988**, *971*, 136.
- (10) Ye, C.; Minami, N.; Marks, T. J.; Yang, J.; Wong, G. K. *Mater. Res. Soc. Symp. Proc.* **1988**, *109*, 263.
- (11) Torruellas, W. E.; Zaroni, R.; Marques, M. B.; Stegeman, G. I.; Mohlmann, G. R.; Erdhuisen, E. W. P.; Horsthuis, W. H. G. *Chem. Phys. Lett.* **1990**, *175*, 267.
- (12) Torruellas, W. E.; Zaroni, R.; Stegeman, G. I.; Moehlmann, G. R.; Erdhuisen, E. W. P.; Horsthuis, W. H. G. *J. Chem. Phys.* **1991**, *94*, 6851.
- (13) Torruellas, W. E.; Zaroni, R.; Stegeman, G. I.; Moehlmann, G. R.; Erdhuisen, E. W. P.; Horsthuis, W. H. G. *J. Chem. Phys.* **1992**, *96*, 1662.

- (14) Mohlmann, G. R.; Horsthuis, W. H. G.; Van der Vorst, C. P. J. M.; McDonach, A.; Copeland, M.; Duchet, C.; Fabre, P.; Diemeer, M. B. J.; Trommel, E. S.; et al. *Proc. SPIE-Int. Soc. Opt. Eng.* **1990**, *1147*, 245.
- (15) Otomo, A.; Stegeman, G. I.; Bosshard, C.; Mittler-Neher, S.; Horsthuis, W. H. G.; Mohlmann, G. R. *Mater. Res. Soc. Symp. Proc.* **1994**, *328*, 631.
- (16) Otomo, A.; Stegeman, G. I.; Horsthuis, W. H. G.; Moehlmann, G. R. *Appl. Phys. Lett.* **1994**, *65*, 2389.
- (17) Otomo, A.; Stegeman, G. I.; Horsthuis, W.; Mohlmann, G. *ACS Symp. Ser.* **1995**, *601*, 469.
- (18) Otomo, A.; Stegeman, G. I.; Horsthuis, W. H. G.; Mohlmann, G. R. *Appl. Phys. Lett.* **1996**, *68*, 3683.
- (19) Otomo, A.; Stegeman, G. I.; Flipse, M. C.; Diemeer, M. B. J.; Horsthuis, W. H. G.; Mohlmann, G. R. *J. Opt. Soc. Am. B* **1998**, *15*, 759.
- (20) Marques, M. B.; Assanto, G.; Stegeman, G. I.; Moehlmann, G. R.; Erdhuisen, E. W. P.; Horsthuis, W. H. G. *Appl. Phys. Lett.* **1991**, *58*, 2613.
- (21) Mittler-Neher, S.; Otomo, A.; Stegeman, G. I.; Bosshard, C.; Horsthuis, W. H. G.; Moehlmann, G. R. *Adv. Mater.* **1995**, *7*, 463.
- (22) Beljonne, D.; Bredas, J. L.; Cha, M.; Torruellas, W. E.; Stegeman, G. I.; Hofstraat, J. W.; Horsthuis, W. H. G.; Moehlmann, G. R. *J. Chem. Phys.* **1995**, *103*, 7834.
- (23) Cha, M.; Torruellas, W. E.; Stegeman, G. I.; Horsthuis, W. H. G.; Mohlmann, G. R.; Meth, J. *Appl. Phys. Lett.* **1994**, *65*, 2648.
- (24) Lee, M. H.; Lee, H. J.; Oh, M. C.; Ahn, J. H.; Han, S. G. *Han'guk Chaelyo Hakhoechi* **1999**, *9*, 355.
- (25) Lee, M.-H.; Lee, H.-J.; Oh, M.-C.; Ahn, J.-H.; Han, S. G.; Kim, H. G. *J. Korean Phys. Soc.* **1999**, *35*, S295.
- (26) Harper, A. W.; Wang, F.; Chen, J.; Lee, M.; Dalton, L. R. *ACS Symp. Ser.* **1999**, *726*, 160.
- (27) Ma, H.; Jen, A. K. Y.; Wu, J.; Wu, X.; Liu, S.; Shu, C.-F.; Dalton, L. R.; Marder, S. R.; Thayumanavan, S. *Chem. Mater.* **1999**, *11*, 2218.
- (28) Ma, H.; Wang, X.; Wu, X.; Liu, S.; Jen, A. K. Y. *Macromolecules* **1998**, *31*, 4049.
- (29) Otomo, A.; Bosshard, C.; Mittler-Neher, S.; Stegeman, G. I.; Kupfer, M.; Florsheimer, M.; Gunter, P.; Horsthuis, W. H. G.; Mohlmann, G. R. *Mol. Cryst. Liq. Cryst. Sci. Technol., Sect. B* **1995**, *10*, 331.
- (30) Dobler, M.; Weder, C.; Ahumada, O.; Neuenschwander, P.; Suter, U. W.; Follonier, S.; Bosshard, C.; Gunter, P. *Macromolecules* **1998**, *31*, 7676.
- (31) Huang, D.; Zhang, C.; Dalton, L. R.; Weber, W. P. *J. Polym. Sci., Part A: Polym. Chem.* **2000**, *38*, 546.
- (32) Wu, B.; Xu, C.; Dalton, L. R.; Kalluri, S.; Shi, Y.; Steier, W. H. *Mater. Res. Soc. Symp. Proc.* **1994**, *328*, 529.
- (33) Xu, C.; Wu, B.; Dalton, L. R. *Proc. SPIE-Int. Soc. Opt. Eng.* **1993**, *1852*, 198.
- (34) Xu, C.; Wu, B.; Becker, M. W.; Dalton, L. R.; Ranon, P. M.; Shi, Y.; Steier, W. H. *Chem. Mater.* **1993**, *5*, 1439.
- (35) Ranon, P. M.; Shi, Y.; Steier, W. H.; Xu, C.; Wu, B.; Dalton, L. R. *Appl. Phys. Lett.* **1993**, *62*, 2605.
- (36) Xu, C.; Wu, B.; Dalton, L. R.; Ranon, P. M.; Shi, Y.; Steier, W. H. *Macromolecules* **1992**, *25*, 6716.
- (37) Kalluri, S.; Steier, W. H.; Xu, C.; Wu, B.; Becker, M. W.; Yang, Z.; Dalton, L. R.; Shi, Y.; Bechtel, J. H. *IEEE Nonlinear Opt.: Mater., Fundam., Appl.* **1994**, 191.
- (38) Sandhya, K. Y.; Pillai, C. K. S.; Sato, M.; Tsutsumi, N. *J. Polym. Sci., Part A: Polym. Chem.* **2003**, *41*, 1527.
- (39) Doeblner, M.; Weder, C.; Ahumada, O.; Neuenschwander, P.; Suter, U. W.; Follonier, S.; Bosshard, C.; Gunter, P. *Macromolecules* **1998**, *31*, 7676.
- (40) Wright, M. E.; Mullick, S. *Macromolecules* **1992**, *25*, 6045.
- (41) Mitchell, M. A.; Mulvaney, J. E.; Hall, H. K., Jr.; Willand, C. S.; Hampsch, H.; Williams, D. J. *Polym. Bull.* **1992**, *28*, 381.
- (42) Stenger-Smith, J. D.; Zarras, P.; Hollins, R. A.; Chafin, A. P.; Merwin, L. H.; Yee, R.; Lindsay, G. A.; Herman, W. N.; Gratz, R. F.; Nickel, E. G. *J. Polym. Sci., Part A: Polym. Chem.* **2000**, *38*, 2824.
- (43) Hayden, L. M.; Kim, W.-K.; Chafin, A. P.; Lindsay, G. A. *J. Polym. Sci., Part B: Polym. Phys.* **2001**, *39*, 895.
- (44) Luo, J.; Qin, J.; Kang, H.; Ye, C. *Polym. Int.* **2000**, *49*, 1302.
- (45) Chen, M.; Yu, L.; Dalton, L. R.; Shi, Y.; Steier, W. H. *Macromolecules* **1991**, *24*, 5421.
- (46) Dalton, L. R.; Wu, B.; Harper, A. W.; Ghosn, R.; Ra, Y.; Liang, Z.; Montgomery, R.; Kalluri, S.; Shi, Y.; et al. *ACS Symp. Ser.* **1995**, *601*, 158.
- (47) Ra, Y. S.; Mao, S. S. H.; Wu, B.; Guo, L.; Dalton, L. R.; Chen, A.; Steier, W. H. *ACS Symp. Ser.* **1998**, *695*, 288.
- (48) Mao, S. S. H.; Ra, Y. S.; He, M.; Zhu, J.; Zheng, C.; Harper, A.; Dalton, L. R.; Gamer, S.; Steier, W. H. *Polym. Mater. Sci. Eng.* **1997**, *77*, 564.
- (49) Shi, Y.; Ranon, P. M.; Steier, W. H.; Xu, C.; Wu, B.; Dalton, L. R. *Proc. SPIE-Int. Soc. Opt. Eng.* **1993**, *2025*, 106.
- (50) Jungbauer, D.; Reck, B.; Twieg, R.; Yoon, D. Y.; Wilson, C. G.; Swalen, J. D. *Appl. Phys. Lett.* **1990**, *56*, 2610.
- (51) Dalton, L. R.; Xu, C.; Wu, B.; Harper, A. W. *Proceedings of the 2nd International Conference on Frontiers in Polymer Advanced Materials* **1994**, 175.
- (52) Li, D.; Marks, T. J.; Zhang, C.; Yang, J.; Wong, G. K. *Proc. SPIE-Int. Soc. Opt. Eng.* **1990**, *1337*, 341.
- (53) Facchetti, A.; Abbotto, A.; Beverina, L.; van der Boom, M. E.; Dutta, P.; Evmenenko, G.; Marks, T. J.; Pagani, G. A. *Chem. Mater.* **2002**, *14*, 4996.
- (54) Facchetti, A.; Abbotto, A.; Beverina, L.; van der Boom, M. E.; Marks, T. J.; Pagani, G. A. *Polym. Prepr. (Am. Chem. Soc., Div. Polym. Chem.)* **2003**, *44*, 1171.
- (55) Keinan, S.; Ratner, M. A.; Marks, T. J. *Chem. Mater.* **2004**, *16*, 1848.
- (56) Marks, T. J.; Ho, S. T.; Liu, Z.; Zhu, P.; Sun, D.-G.; Ma, J.; Xiao, Y.; Kang, H. *Proc. SPIE-Int. Soc. Opt. Eng.* **2003**, *4991*, 133.
- (57) Zhu, P.; Kang, H.; Facchetti, A.; Evmenenko, G.; Dutta, P.; Marks, T. J. *J. Am. Chem. Soc.* **2003**, *125*, 11496.
- (58) Shin, D. M.; Whitten, D. G. *J. Am. Chem. Soc.* **1988**, *110*, 5206.
- (59) Cahill, P. A.; Seager, C. H.; Meinhardt, M. B.; Beuhler, A. J.; Wargowski, D. A.; Singer, K. D.; Kowalczyk, T. C.; Kosci, T. Z. *Proc. SPIE-Int. Soc. Opt. Eng.* **1993**, *2025*, 48.
- (60) Matyushov, D. V.; Schmid, R. *J. Phys. Chem.* **1994**, *98*, 5152.
- (61) Matyushov, D. V.; Schmid, R. *Mol. Phys.* **1995**, *84*, 533.
- (62) Lilichenko, M.; Matyushov, D. V. *J. Phys. Chem. B* **2003**, *107*, 1937.
- (63) Milischuk, A.; Matyushov, D. V. *J. Chem. Phys.* **2003**, *118*, 5596.
- (64) Abdel Mottaleb, M. S. A.; Sherief, A. M. K. *Z. Phys. Chem. (Leipzig)* **1984**, *265*, 154.
- (65) Kuder, J. E.; Wychick, D. *Chem. Phys. Lett.* **1974**, *24*, 69.
- (66) Skumanich, A. *Mater. Res. Soc. Symp. Proc.* **1992**, *228*, 85.
- (67) Kristjansson, I.; Ulstrup, J. *Chem. Scr.* **1985**, *25*, 49.
- (68) Shin, D. M.; Schanze, K. S.; Otruba, J. P.; Brown, P. E.; Whitten, D. G. *Isr. J. Chem.* **1988**, *28*, 37.
- (69) Meeder, A.; Fuertes Marron, D.; Chu, V.; Conde, J. P.; Jager-Waldau, A.; Rumberg, A.; Lux-Steiner, M. C. *Thin Solid Films* **2002**, *403*–*404*, 495.
- (70) Abate, J. A.; Roides, R. *J. Phys., Colloq.* **1983**, 497.
- (71) Aljishi, S.; Smith, Z. E.; Chu, V.; Kolodzey, J.; Slobodin, D.; Conde, J. P.; Shen, D. S.; Wagner, S. *AIP Conf. Proc.* **1987**, *157*, 25.
- (72) Amato, G.; Fizzotti, F. *Phys. Rev. B: Condens. Matter Mater. Phys.* **1992**, *45*, 14108.
- (73) Boulitrop, F.; Bullot, J.; Gauthier, M.; Schmidt, M. P.; Catherine, Y. *Solid State Commun.* **1985**, *54*, 107.
- (74) Mullins, O. C.; Mitra-Kirtley, S.; Zhu, Y. *Appl. Spectrosc.* **1992**, *46*, 1405.
- (75) Tanaka, K.; Gotoh, T.; Yoshida, N.; Nonomura, S. *J. Appl. Phys.* **2002**, *91*, 125.
- (76) Barto, R. R.; Frank, C. W.; Ermer, S. P.; Anderson, W. W.; Sun, S.-S.; Maaref, S.; Jen, A. K. Y.; Luo, J. D.; Lee, M. *Proc. SPIE-Int. Soc. Opt. Eng.* **2002**, *4823*, 54.
- (77) Rosencwaig, A.; Gersho, A. *J. Appl. Phys.* **1976**, *47*, 64.